

physica **p** status **s** solidi **S**

www.interscience.wiley.com

reprints

The collage features five journal covers:

- physica status solidi **a**** (www.pss-a.com): Applications and materials science. Editor's Choice: Highly efficient all-nitride phosphor-converted white light emitting diode (Regina Mueller-Mach et al., p. 1727). Includes a diagram of a light-emitting diode structure.
- physica status solidi **b**** (www.pss-b.com): Basic solid state physics. Current Trends in Electronic Structure: Embedding and Linear Scaling Techniques (Thomas Beck, and Eduardo Hernandez). Includes a diagram of a crystal lattice.
- physica status solidi **c**** (www.pss-c.com): Current topics in solid state physics. Includes a photograph of a glowing material.
- physica status solidi **rrl**** (www.pss-rapid.com): Rapid research letters. Includes a diagram of a crystal structure.
- physica status solidi **a**** (www.pss-a.com): Applications and materials science. Includes a diagram of a light-emitting diode structure.

Additional text on the collage includes "SPECIAL ISSUE" and "www.pss-rapid.com".

Characterization of chemical bath deposited buffer layers for thin film solar cell applications

D. Dwyer¹, R. Sun², H. Efsthadiadis¹, and P. Haldar^{*1}

¹ College of Nanoscale Science and Engineering, University at Albany – State University of New York, 257 Fuller Rd., Albany, NY 12203, USA

² Angstrom Sun Technologies Inc., 33 Nagog Park, Acton, MA 01720, USA

Received 11 October 2009, revised 28 January 2010, accepted 16 April 2010

Published online 24 June 2010

Keywords absorption spectra, compound semiconductors, solar cells

* Corresponding author: e-mail phaldar@uamail.albany.edu, Phone: 1 518 437 8684, Fax: +1 518 437 8687

Cadmium sulfide (CdS), indium sulfide (In₂S₃) and zinc sulfide (ZnS) thin films have been deposited by chemical bath deposition (CBD) for buffer layer applications in Cu–chalcopyrite-based thin film solar cells. Films were characterized by scanning electron microscopy (SEM), UV–Vis transmission, X-ray photoelectron spectroscopy (XPS), grazing-incidence X-ray diffraction (GIXRD), and spectroscopic

ellipsometry. Results indicate CdS can be deposited with low oxygen content and high light transmission over 245–1700 nm. CBD-ZnS and CBD-InS both exhibit 5–10% less light transmission than CdS in the same thickness range. In terms of light transmission and degree of impurities CdS appears to be a better buffer material than CBD-ZnS or CBD-InS.

© 2010 WILEY-VCH Verlag GmbH & Co. KGaA, Weinheim

1 Introduction CuInGaSe₂ (CIGS) thin film solar cells have demonstrated efficiencies approaching 20% [1]. The typical CIGS device consists of soda-lime glass (SLG)/Mo/CIGS/CdS/i-ZnO/ZnO:Al/Ni–Al grid device stack. The cadmium sulfide (CdS) in this stack is usually deposited by chemical bath deposition (CBD). While CBD is an inexpensive and relatively easy process to form thin continuous films, the resulting toxic cadmium-containing waste is an issue. The economic and environmental impact of this process step is magnified as large volume production begins, and work must be focused on a viable alternative that can be easily integrated into existing production lines [2].

For a material to be a suitable buffer layer a few requirements must be met. First a high band gap is desired, with high light transmission below the band edge to allow maximum light generated current. CdS has a band gap of ~2.4 eV, corresponding to a photon wavelength of 517 nm. Photons with energy above 2.4 eV can be optically absorbed, reducing the available light to generate electron–hole pairs in the absorber layer. A higher band gap film that allows light transmission down to 370 nm (~3.35 eV) is desired. Second, films must form a continuous coating over the absorber layer

at low thicknesses. Pinholes in the film can cause localized degradation in electronic properties, increasing tunneling and lowering contact potential at the junction [3]. This continuous coating must be formed at low thicknesses (<100 nm) to avoid losses in light transmission associated with thicker films.

The conduction band offset (CBO) that is created at the CIGS/buffer interface is also important, especially for wide band gap absorber materials for both single and multi-junction devices. The CBO of the highest efficiency CIGS cells (band gap ~1.15 eV) at the CIGS/CdS interface is ~0.3 eV. This is a nearly optimal value. As the absorber band gap is increased buffers with wider band gaps than CdS are needed to maintain this ideal CBO value [4, 5].

Numerous alternatives to CdS have been studied using a both wet chemical and dry deposition methods [6, 7]. Of these deposition methods, only atomic layer deposition (ALD) and CBD are able to produce conformal films over rough surfaces on the order of 20–100 nm. These methods have also shown the highest efficiency results [7]. The deposition speed of a CBD process is faster than an ALD process, and is already being implemented in manufacturing lines, so we focus our work on this process.

© 2010 WILEY-VCH Verlag GmbH & Co. KGaA, Weinheim

CBD-zinc sulfide (ZnS) and CBD-InS have demonstrated the highest efficiencies of alternative buffers to this point, both approaching efficiencies of similar absorbers buffered with CdS. Device efficiencies of 18.6% for CBD-ZnS and 15.7% for CBD-InS have been recorded [8, 9].

The CBD of these materials generally consists of a sulfur source, a complexing agent, and a compound containing Cd, In, or Zn. For this study, the standard NREL CdS deposition procedure developed by Contreras et al. [3] was used. Here cadmium sulfate (CdSO_4) is the cadmium source, thiourea (NH_2CSNH_2) is the sulfur source, and ammonium hydroxide (NH_4OH) acts as the complexing agent.

The method developed by Nakada was used for ZnS depositions. The resulting films are actually expected to be a combination of ZnS, $\text{Zn}(\text{OH})_2$, and ZnO, but will be referred to as CBD-ZnS. Here zinc sulfate (ZnSO_4) is the zinc source, thiourea (NH_2CSNH_2) is the sulfur source, and ammonia is the complexing agent [10].

Indium sulfide was deposited using the method developed by Hariskos et al. [9]. Similar to CBD-ZnS, a large degree of oxygen is present in these films forming a $\text{In}_x(\text{OH},\text{S})_y$ compound we refer to as CBD-InS. In this procedure indium chloride (InCl_3) is the indium source, and thioacetamide (CH_3CSNH_2) the sulfur source. No complexing agent is used.

For this paper, these three buffer films were deposited by CBD so that the basic materials properties and growth behavior of CBD-ZnS and CBD-InS could be compared to the current standard CdS film. Using a variety of characterization techniques the optical, crystallographic, and chemical properties of these three films were measured, and the results will be discussed.

2 Experimental procedure

2.1 Deposition of buffer films All films in this work were deposited by CBD. An exterior bath, heated by a hot plate, was used to evenly distribute the temperature around a 1000 mL deposition beaker. Samples were held vertically by Teflon clamps, and stirring was maintained at 350 rpm. For all depositions both a SLG and molybdenum-coated soda-lime glass (Mo/SLG) substrate were used. Once depositions were complete samples were rinsed in a DI water bath and dried with nitrogen.

Table 1 shows the deposition conditions used to create films of similar thickness, with a target of 50–100 nm. For

CdS samples the deposition time could be used to vary thickness. For both CBD-InS and CBD-ZnS it was found that thickness could not be varied significantly by increasing deposition time. To increase the thickness of these films multiple depositions were run using the same CBD conditions, and each single deposition is referred to as a dip.

For CdS depositions the exterior water bath was heated to 65 °C. Once the exterior bath was at temperature 50 mL of 0.015 M CdSO_4 , 25 mL of 1.5 M thiourea (NH_2CSNH_2), 62.5 mL of ammonium hydroxide (NH_4OH) (28–30% w/w), and 366 mL of DI water were added to the beaker. Samples were then added and depositions were run for 13–21 min.

For CBD-ZnS films, 213 mL of 7.5 M ammonia and 287 mL of DI water were heated to a temperature of 80 °C. For this deposition, as well as CBD-InS, the thermocouple was placed into the deposition beaker itself. A pH strip was used to ensure a bath pH of ~ 11 . 29.88 g ZnSO_4 and 22.84 g thiourea (NH_2CSNH_2) were added once the bath reached temperature, and samples were added once the chemicals dissolved. Depositions were run for 15 min, and multiple dips were used to increase sample thickness.

CBD-InS depositions began by heating 500 mL of DI water to 70 °C. 0.553 g InCl_3 and 5.635 g thioacetamide (CH_3CSNH_2) were added once the bath reached temperature. Samples were added after adding the chemicals and the depositions were run for 20 min. The pH of this bath began at ~ 3.4 and decreased to 3 as the deposition progressed. Multiple dips were used to increase sample thickness.

2.2 Film characterization Film surface morphology was imaged using a Carl Zeiss 1550 Schottky source electron microscope operating at 5 kV. The low accelerating voltage was used to provide a more surface sensitive image. Films deposited on Mo coated substrates were used to prevent charging.

Film surface characterization and compositional depth profiles were measured using X-ray photoelectron spectroscopy (XPS). The XPS surface characterization and sputter depth profiling were performed using a ThermoVG Thetaprobe equipped with a hemispherical analyzer and a monochromated Al K α X-ray source (1486.6 eV) operated at a 100 W/400 mm spot mode for area-averaged analyses. Pass energy for surveys and depth profiles were 300 and 125 eV, respectively. Sputter depth profiling was accomplished using an argon ion gun operated at 2.5 keV with a sample current of

Table 1 Summary of film deposition parameters and resulting thicknesses determined by spectroscopic ellipsometry.

sample ID	material stack	deposition time (min)	number of dips in bath	thickness (nm)
CdS-1	CdS/Mo/glass	15	1	17 + 1
CdS-2	CdS/Mo/glass	17	1	36 + 3
CdS-3	CdS/Mo/glass	21	1	60 + 3
InS-1	InS/Mo/glass	20	1	4 + 1
InS-2	InS/Mo/glass	20	2	24 + 1
InS-3	InS/Mo/glass	20	3	66 + 4
ZnS-1	ZnS/Mo/glass	15	1	72 + 3
ZnS-2	ZnS/Mo/glass	15	2	200 + 6

~1.2 mA, yielding a sputter rate of 4 nm/min for SiO₂. The XPS chamber was maintained at 2×10^{-9} Torr during analysis, except during argon introduction.

A Woollham Dual Rotating Compensator with a quartz tungsten halogen and deuterium lamp was used to measure transmission curves from 245 to 1700 nm. From this data the absorption coefficients (α) were determined using the equation:

$$I_T = I_0 e^{(-\alpha t)}, \quad (1)$$

where t is the film thickness, α the absorption coefficient, I_T the intensity of transmitted light, and I_0 is the intensity of initial light. The optical band gap is related to the absorption coefficient by:

$$\alpha = \frac{K(h\nu - E_g)^n}{h\nu}, \quad (2)$$

where K is a constant, E_g the optical band gap, n is taken as 1/2 for direct band gap materials or 2 for indirect band gap materials, and $h\nu$ is the photon energy. Using the calculated absorption coefficients plots of $(\alpha h\nu)^2$ versus $h\nu$ (direct band gap), and $(\alpha h\nu)^{1/2}$ versus $h\nu$ (indirect band gap) were produced. The x -axis intercept of a linear fit to each plot was used to estimate the optical band gap of films. It is important to note that these calculations do not account for possible interference effects from reflection, which are assumed to be minimal due to the low film thicknesses.

XRD scans were carried out on a Scintag X-ray diffractometer equipped with a Cu K α X-ray source and a horizontal wide-angle four-axis goniometer with stepping motors which allowed independent or coupled $\theta/2\theta$ axes motion. XRD spectra were collected at a grazing-incidence (GIXRD) ω of 2°. The collected GIXRD patterns were compared to reference patterns from the standard joint committee for powder diffraction standards (JCPDS) powder diffraction file (PDF).

The average crystalline grain size D was estimated using Scherrer formula

$$D = \frac{0.94\lambda}{\beta \cos(\theta)}, \quad (3)$$

where λ is the X-ray wavelength, β the full width at half maximum (FWHM) of the diffraction peak in radians, θ the Bragg angle, and 0.94 is the shape factor for cubic crystals [11].

An Ellipsometer, Model TFProbe SE200BA, made by Angstrom Sun Technologies, Inc., was used to determine film thickness and optical constants for prepared films. Spectroscopic ellipsometry is a non-contact, non-destructive, and optical technique. Its principle in determining physical and optical properties is based on matching modeling by comparing measured ellipsometry parameters, Psi (Ψ) and Del (Δ), with theoretical calculated set of parameters with assumed models. Here Ψ is defined by the

equation

$$\tan(\Psi) = \left| \frac{R^P}{R^S} \right|, \quad (4)$$

where R^P is the parallel reflected component and R^S is the perpendicular reflected component. Δ is the phase difference after reflection, $\delta_1 - \delta_2$.

TFProbe SE200BA spectroscopic ellipsometer covers a wavelength range from 250 to 850 nm and has advanced automatically variable incident angle functions. All samples were measured at 65, 70, and/or 75° of incident angles with 256 wavelength points. Measured data sets were then modeled with TFProbe 3.2 version software. The Tauc-Lorentz model is used for obtaining optical functions of films in which the imaginary part of the dielectric function ϵ_i is determined by multiplying the Tauc joint density of states by the ϵ_i obtained from the Lorentz oscillator model:

$$\epsilon_i(E) = \frac{AE_0 C(E - E_g)^2}{((E^2 - E_0)^2 + C^2 E^2)E}, \quad E > E_g, \quad (5)$$

$$\epsilon_i(E) = 0, \quad E \leq E_g,$$

where E_0 is the peak transition energy, C the broadening term, E_g the optical band gap, and A is proportional to the transition probability matrix element [12].

The real part of the dielectric function ϵ_r is obtained by Kramers-Kronig integration:

$$\epsilon_r(E) = \epsilon_r(\infty) + \frac{2P}{\pi} \int_{E_g}^{\infty} \frac{\xi \epsilon_i(\xi)}{\xi^2 - E^2} d\xi, \quad (6)$$

Thus A , C , E_0 , E_g and E_{inf} are treated as fitting parameters in software.

3 Results and discussion A summary of sample deposition parameters and their resulting thicknesses can be seen in Table 1. Increasing deposition time increased the thickness of CdS films, however, both zinc and indium sulfide films did not show any significant increases in thickness with additional deposition time. It is believed in the case of CBD-ZnS this is due to a depletion of the reactants, as the film grows approximately the same thickness in each deposition.

For CBD-InS films sub-10 nm thicknesses were still found after 30 min of reaction time, whereas samples dipped multiple times show a non-linear increase in thickness. The sharp increase in thickness in the subsequent dips is likely due to an increased film growth rate on the In_x(O,H)_y-In₂S₃/Mo/SLG substrate versus the Mo/SLG substrate. In the first deposition by the time the initial layer is formed, much of the bath has reacted in solution. During the second and third dips the reaction is able to occur on the In_x(O,H)_y-In₂S₃ surface before being depleted in the solution, leading to a faster deposition rate.

3.1 Film morphology Each CdS, CBD-ZnS, and CBD-InS film on Mo/SLG was characterized by top-view scanning electron microscopy (SEM) to compare the surface morphology of the different films.

Figure 1 shows the progression of CdS film growth with deposition time, starting with a bare Mo film surface. At 13 min CdS grains have begun to nucleate on the Mo grains. These clusters appear to be ~ 40 nm in diameter and continue to grow to 50–60 nm at 15 min. At ~ 19 min the film has coalesced into a continuous coating. This corresponds to a thickness of ~ 40 –50 nm, and the interference pattern on the Mo produces deep blue/purple coloration. It appears that a heterogeneous reaction occurs, forming colloids that adhere to the roughest areas of the substrate, which are the Mo grains in this case. After this initial attachment films grow laterally filling in the voids between colloids.

Top-view images of CBD-InS and CBD-ZnS are shown in Fig. 2. After one dip the CBD-ZnS sample was found to be ~ 70 nm, however, at this thickness a low density of pinholes was still seen. Samples dipped twice were pinhole free. Samples were also found to have a secondary layer of particles over areas of the film, however, these could be removed by sonicating the films in DI water. These films seem to initially grow by a similar colloidal mechanism as CdS. However, rather than the voids being filled laterally, the growth rate of CBD-ZnS grains appears to be equivalent in all directions resulting in thicker films. It is important to note that others have found continuous CBD-ZnS films grown on CIGS at thicknesses of < 50 nm, however, peak efficiencies were found to occur for 100–150 nm thick films [10, 13].

CBD-InS films were only ~ 4 –5 nm after one dip for 20 min. Visually this ultra-thin film appears to be continuous over the entire substrate, resulting in a light brown tint on the Mo/SLG substrate. The second and third dips thickened the film and the platelet-like growth continued.

3.2 Crystallinity GIXRD spectra were taken from CdS-3, InS-3, and ZnS-2 films. CdS and CBD-ZnS were polycrystalline with CdS favoring the (111) peak and CBD-ZnS favoring the (311) peak, both with a cubic structure. CBD-InS was found to be amorphous. This explains the apparent lack of structure observed in the CBD-InS SEM

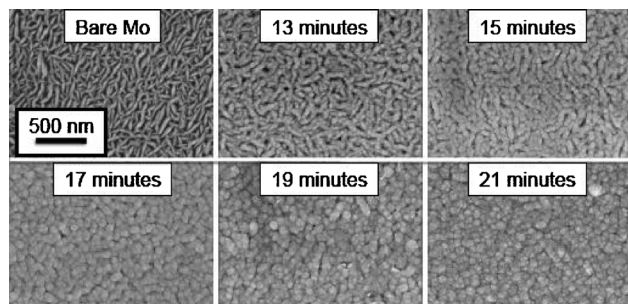


Figure 1 Top-view SEM images of CdS/Mo/SLG films. At 13 min colloidal particles have deposited on Mo surface features. By 19 min a continuous and pinhole free film has formed.

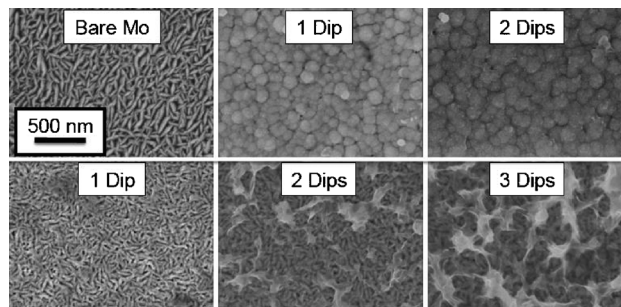


Figure 2 Top-view SEM images of CBD-ZnS/Mo/SLG (top row) and CBD-InS/Mo/SLG (bottom row), with a bare Mo film for comparison. Film thicknesses increase from left to right.

images. Similar amorphous CBD-InS has been found by others as well [14].

The grain size of the crystalline films was estimated with the Scherrer formula using the (220) peak for CdS calculations, and (311) peak for CBD-ZnS. The grain size for CdS-3 was estimated to be 16 nm, while ZnS-2 was estimated to be 22 nm. No direct correlation has been found between grain size and final device performance, however, in the case of CdS films there is a correlation between grain size and band gap. Band gap energy was found to increase from ~ 2.35 to 2.47 eV with grain size decreasing from ~ 200 Å down to 85 Å due to quantum effects [11]. Increasing the CdS band gap by reducing grain size should increase light generated current in the absorber.

3.3 Film composition XPS compositional depth profiles are seen in Fig. 3. CdS was found to have a Cd:S ratio of ~ 1.2 , with 3–4% oxygen present in the bulk. The slight sulfur deficiency is expected in CBD CdS films, and has in the past been attributed to other by-product cadmium compounds of the CBD reaction coexisting with the CdS [15]. Significant carbon and oxygen are present at the surface but are removed by sputtering. No nitrogen or OH-compounds were found in the film surface or bulk.

CBD ZnS data indicates a Zn:S ratio of ~ 1.8 , with 20–30% oxygen in the film. A high-energy shoulder on the oxygen peak at ~ 533.3 eV was found at the film surface, and decreasing into the bulk suggesting the presence of $\text{Zn}(\text{OH})_2$. This presence of oxygen has been explained by the equilibrium chemistry of the solution. There appears to be a competition between the formation of the sulfide and hydroxide in basic solutions, where the solubility product equilibrium constant (K_{sp}) for $\text{Zn}(\text{OH})_2$ is $10^{-15.3}$ and $10^{-23.8}$ for ZnS [16]. The smaller the K_{sp} value the larger the concentration of reactant compared to products, i.e., fewer products produced.

The sulfur appears to increase toward the substrate while the oxygen decreases, which is likely a result of variation in the bath sulfur content as the deposition proceeds [17]. Nitrogen is not found throughout the entire film thickness, however, a small amount of carbon appears toward the substrate. This could be a result of residue on the Mo

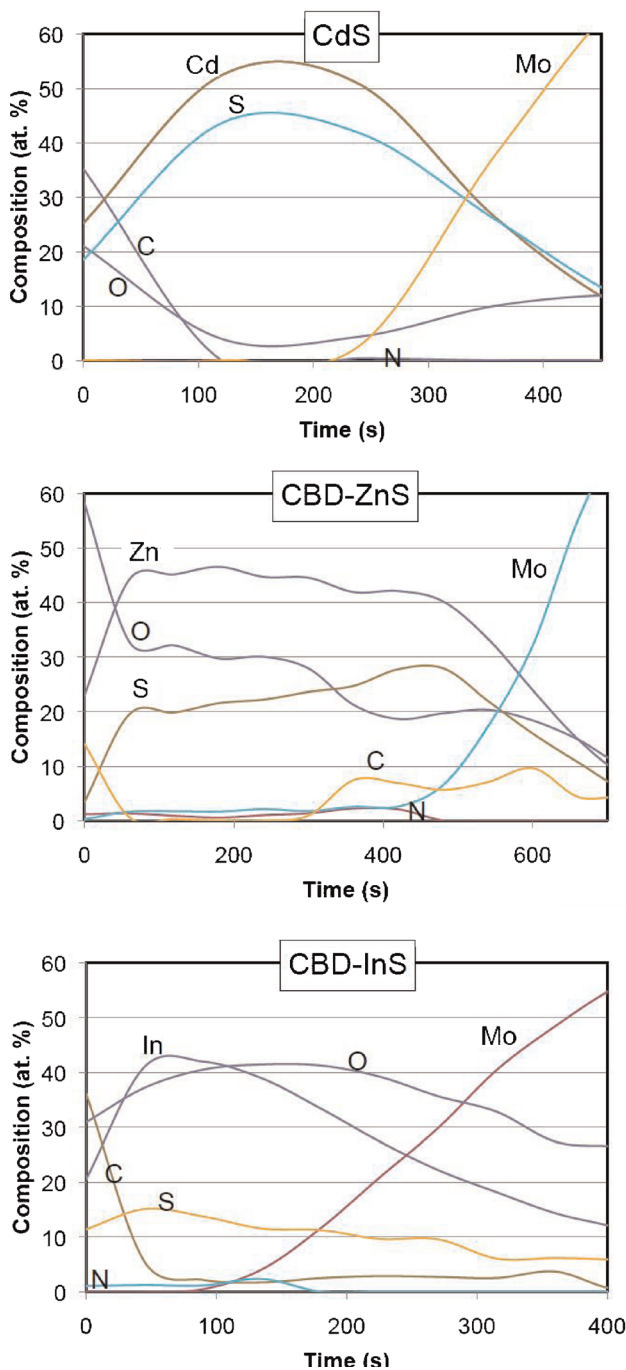


Figure 3 (online color at: www.pss-a.com) XPS compositional depth profiles of (a) CdS/Mo/SLG, (b) CBD-ZnS/Mo/SLG, and (c) CBD-InS/Mo/SLG.

substrate, or impurities from the thiourea (NH_2CSNH_2) deposited during film formation.

XPS of CBD-InS also reveals a large quantity ($\sim 40\%$) of oxygen in the bulk. In this case, only surface $\text{In}_x(\text{OH})_y$ is found, with the oxygen peak shifted to ~ 533 eV. Again no nitrogen is seen, and carbon is limited to the surface. The In:S ratio is ~ 2.7 . If the oxygen and sulfur are added this gives a stoichiometry of $\sim \text{In}_2(\text{O},\text{S})_3$. The films are likely a

combination between indium hydroxide sulfide, indium oxide, and indium sulfide [14].

3.4 Optical measurements

3.4.1 Transmission Figure 4 shows the transmission data from three films with 60–70 nm thicknesses, as well as a thin (24 nm) continuous CBD-InS and a blank glass slide for comparison. CdS is expected to show a sharp decrease in transmission below ~ 517 nm, corresponding to a band gap of 2.4 eV. A small drop in transmission is seen, however, it appears to be minimal at ~ 60 nm thickness. When compared to similar thickness CBD-InS and CBD-ZnS the CdS film appears to have higher transmission over all wavelengths. CBD-ZnS shows higher transmission than CBD-InS above ~ 650 nm, however, below this wavelength the transmission decreases more sharply. The very broad absorption edge of CBD-InS is also in agreement with the amorphous result seen GA-XRD data. CdS appear to have the sharpest edge, followed by CBD-ZnS suggesting a lesser crystallinity in the latter. A thinner CBD-InS is also shown. This film appears to have higher transmission due to its minimal thickness, and could be an effective buffer if it can create in a large enough depletion width to prevent tunneling.

This transmission data were used to produce plots of $(\alpha h\nu)^2$ versus $h\nu$, as well as $(\alpha h\nu)^{1/2}$ versus $h\nu$ to estimate the optical band gaps. Both CdS and CBD-ZnS were found to fit as direct band gaps, while CBD-InS fit as an indirect band gap. The band gap of CdS was found to be 2.34 eV, in agreement with the accepted value of 2.4 eV. The CBD-ZnS was found to have a gap of 3.6 eV, equal to the single crystal value [18]. CBD-InS fit to a band gap of 3.42 eV. Generally observed values have been in the broad range of 2–3.7 eV. CBD deposited samples have tended toward the higher gaps due to the presence of oxygen, and purer physical vapor deposition samples toward the single crystal value of ~ 2 eV [19]. The large oxygen content found in XPS results may explain the wide band gap suggested by the fit. The ability to vary the band gap of CBD-InS by altering bath parameters,

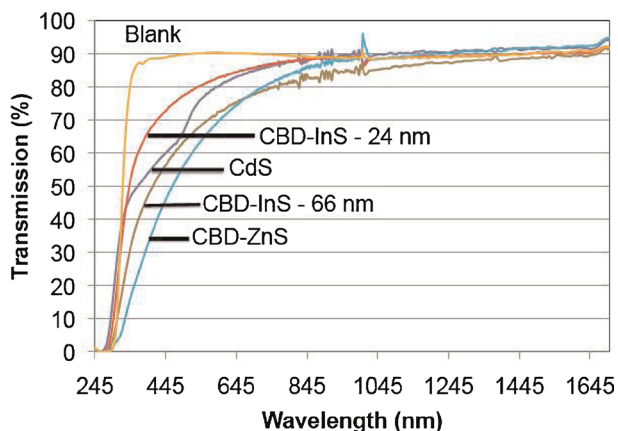


Figure 4 (online color at: www.pss-a.com) Transmission data from CdS-3, CBD-ZnS-1, InS-2, and InS-3 films deposited on SLG. A bare glass substrate is included for comparison.

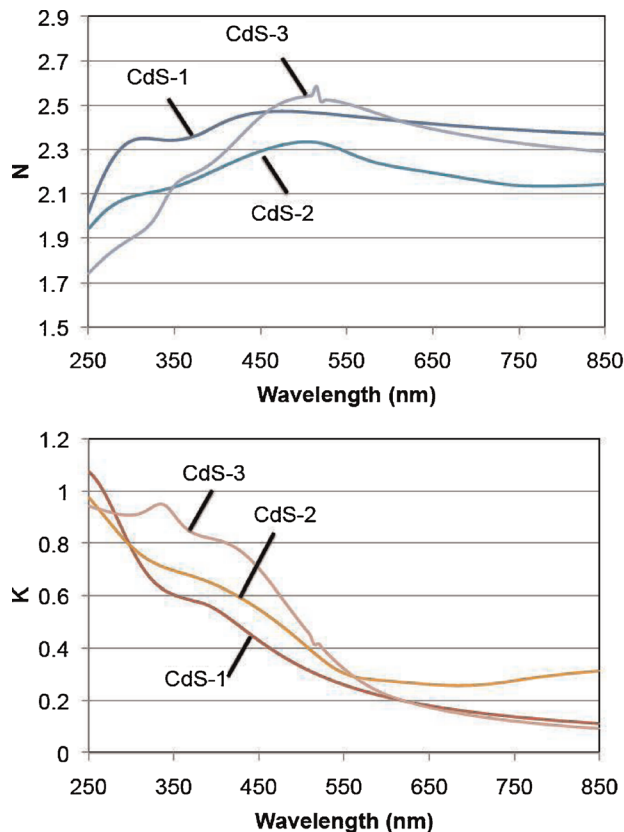
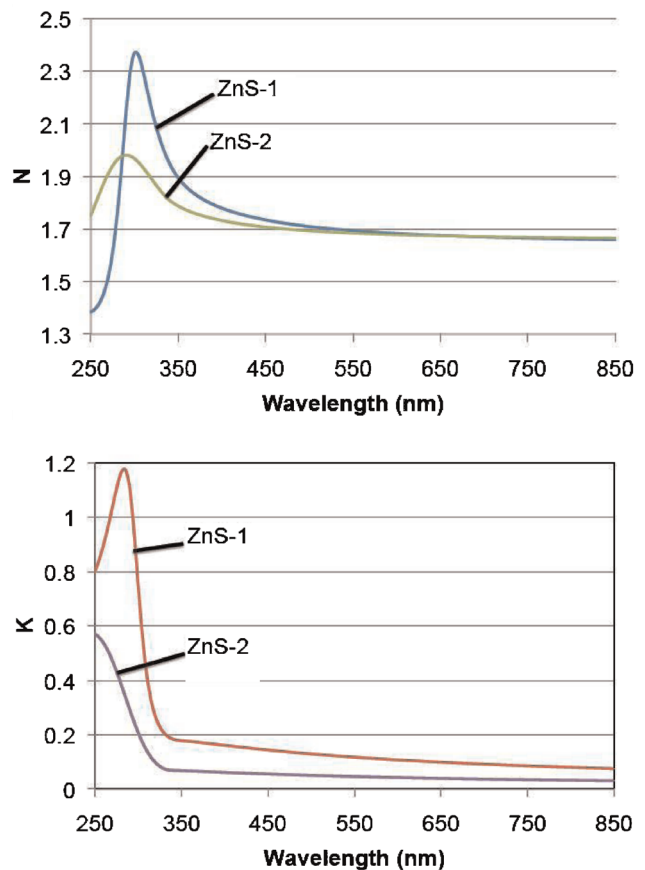
Table 2 Analyzed results from spectroscopic ellipsometer.

sample ID	Tauc-Lorentz parameters					Notes
	A	C	E_0	E_g	E_∞	
CdS-1	2.76	7.66	4.27	1.70	0.72	3 Lorentz bands
CdS-2	2.74	6.59	4.29	2.17	1.07	1 Lorentz band
CdS-3	2.84	7.86	3.93	2.02	1.19	3 Lorentz bands
InS-1	34.03	12.50	4.10	2.39	7.93	1 Lorentz band
InS-2	28.89	12.50	4.10	2.44	5.80	1 Lorentz band
InS-3	4.59	13.00	4.10	2.10	1.90	1 Lorentz band
ZnS-1	0.16	0.51	4.21	3.55	0.241	1 Lorentz band
ZnS-2	0.48	1.61	4.35	3.66	0.08	1 Lorentz band

and in turn the oxygen content, may prove to be an advantage when tailoring the CBO to different band gap absorber films.

3.4.2 Spectroscopic ellipsometry Results obtained with spectroscopic ellipsometer are summarized in Table 2. All data shown were taken from samples deposited on Mo/SLG substrates. Curve fittings were consistent with measured data for all plots.

Optical constant N (refractive index), and K (extinction coefficient) are plotted in Figs. 5–7 for CdS, CBD-ZnS, and CBD-InS, respectively. For samples CdS-1 and CdS-3 additional Lorentzian absorption bands were added into dielectric function to improve fitting. The average optical

**Figure 5** (online color at: www.pss-a.com) Optical constant plots for CdS films.**Figure 6** (online color at: www.pss-a.com) Optical constant plots for CBD-ZnS films.

band gaps obtained from ellipsometry analysis are 2.31, 3.61, and 1.96 eV respectively for CBD-InS, CBD-ZnS, and CdS films.

The peak in the N -spectra for CdS at ~ 450 – 515 nm (2.76–2.41 eV) corresponds to an optical transition at the fundamental absorption edge. There appears to be a shift toward a lower energy transition as the samples become thicker. Another transition associated with the direct gap along the Brillouin zone of the wurtzite CdS lattice at ~ 260 nm (4.77 eV) has been found in previous studies, however, this appears only in our thinnest CdS film [20].

CBD-InS shows a peak in the N -spectra for only the thickest film at ~ 350 nm (3.5 eV). There is also a decrease in refractive index with increasing thickness. This is probably a result of an increase in porosity. An interface may be developing as a result of the multiple dips that are necessary to increase film thickness.

The CBD-ZnS samples show N -spectra peaks at 300 nm (4.13 eV) and 290 nm (4.28 eV) for ZnS-1 and ZnS-2, respectively. The critical point in bulk ZnS is expected around 330 nm [21]. It appears the oxygen incorporated during the CBD process is producing a peak shift, with the thicker sample showing a larger shift. The N value at this peak is also decreased in the thicker sample, indicating the thicker sample is more porous than the thinner sample.

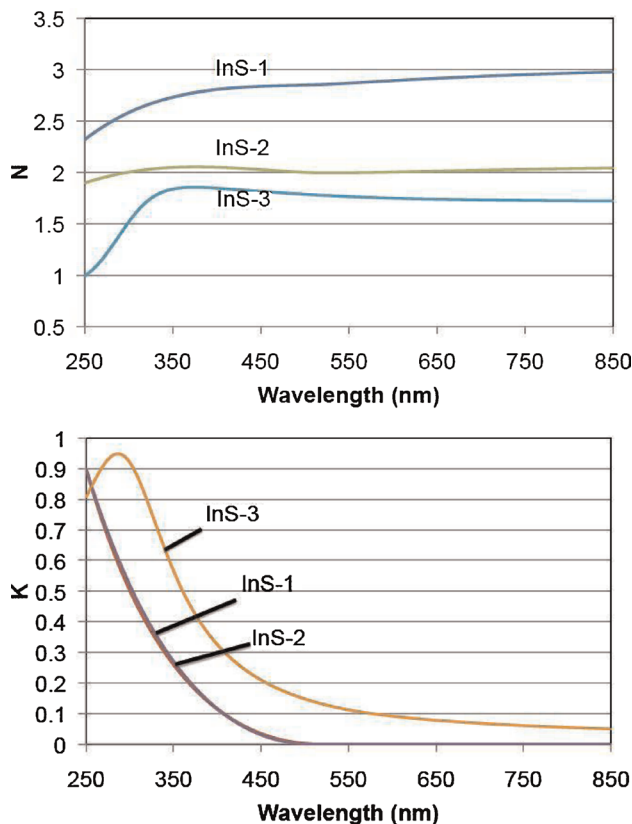


Figure 7 (online color at: www.pss-a.com) Optical constant plots for CBD-InS films.

4 Conclusion CdS, CBD-ZnS, and CBD-InS thin films have been deposited on SLG and Mo\SLG substrates. CBD-InS and CBD-ZnS suffer from poorer light transmission than CdS at similar thicknesses, even with their wider band gaps. They also contain a high degree of oxygen, which would need to be controlled to obtain reproducible results. In this work, we do not take into account the surface passivation and diffusion properties of the buffer layers into the absorber surface region, which will also be influential in determining the final device efficiencies and interface properties.

Based on the film properties studied, the data suggest that CdS is a better buffer choice than CBD-ZnS or CBD-InS due to higher light transmission, smooth surface coverage, and low degree of impurities.

Acknowledgements This research was supported by the New York State Foundation for Science, Technology, and

Innovation (NYSTAR). The authors would like to thank Richard Moore of the College of Nanoscale Science and Engineering (CNSE) for assistance with XPS measurements, as well as Dr. Ingrid Repins of the National Renewable Energy Laboratory (NREL) for useful discussions. We would also like to thank Jeff Wells and Erin Bedford of CNSE for their contributions to this work.

References

- [1] I. Repins, M. A. Contreras, B. Egaas, C. DeHart, J. Scharf, C. Perkins, B. To, and R. Noufi, *Prog. Photovolt.* **16**, 235 (2008).
- [2] K. M. Hynes and J. Newham, in: *Proceedings of the 16th European Photovoltaics Conference*, Glasgow, UK, 2000, p. 2297.
- [3] M. A. Contreras, M. Romero, B. To, F. Hasoon, R. Noufi, S. Ward, and K. Ramanathan, *Thin Solid Films* **403/404**, 204 (2002).
- [4] M. Gloeckler and J. Sites, *Thin Solid Films* **480/481**, 241 (2005).
- [5] A. Pudov, J. R. Sites, M. A. Contreras, T. Nakada, and H.-W. Schock, *Thin Solid Films* **480/481**, 273 (2005).
- [6] S. Siebentritt, *Sol. Energy* **77**, 767 (2004).
- [7] D. Hariskos, S. Spiering, and M. Powalla, *Thin Solid Films* **480/481**, 99 (2005).
- [8] M. A. Contreras, T. Nakada, M. Hongo, A. O. Pudov, and J. R. Sites, in: *Proceedings of the 3rd World Conference of Photovoltaic Energy Conversion*, Osaka, Japan, 2003, p. 570.
- [9] D. Hariskos, M. Ruckh, U. Ruhle, T. Walter, H.-W. Schock, J. Hedstrom, and L. Stolt, *Sol. Energy Mater. Sol. Cells* **41/42**, 345 (2004).
- [10] T. Nakada and M. Mizutani, *Jpn. J. Appl. Phys.* **41**, L165 (2002).
- [11] A. Cortes, H. Gomez, R. E. Marotti, G. Riveros, and E. A. Dalchiele, *Sol. Energy Mater. Sol. Cells* **82**, 21 (2004).
- [12] G. E. Jellison, Jr., *Thin Solid Films* **313/314**, 22 (1998).
- [13] A. Ichiboshi, M. Hongo, T. Akamine, T. Dobashi, and T. Nakada, *Sol. Energy Mater. Sol. Cells* **90**, 3130 (2006).
- [14] N. Barreau, J. C. Bernede, H. El Maliki, S. Marsillac, X. Castel, and J. Pinel, *Solid State Commun.* **122**, 445 (2002).
- [15] C. Guillen, M. A. Martinez, C. Maffiotte, and J. Herrero, *J. Electrochem. Soc.* **148**, 602 (2001).
- [16] B. Mokili, M. Froment, and D. Lincot, *J. Phys. Fr. IV* **5**, C3 (1995).
- [17] M. Bär, A. Ennaoui, J. Klaer, T. Kropp, R. Sáez-Araoz, N. Allsop, I. Laueremann, H.-W. Schock, and M. C. Lux-Steiner, *J. Appl. Phys.* **99**, 123503 (2006).
- [18] B. R. Sankapal, S. D. Sartale, C. D. Lokhande, and A. Ennaoui, *Sol. Energy Mater. Sol. Cells* **83**, 447 (2004).
- [19] N. Barreau, *Sol. Energy Mater. Sol. Cells* **83**, 363 (2009).
- [20] M. G. Sandoval-Paz, M. Sotelo-Lerma, A. Mendoza-Galvan, and R. Ramirez-Bon, *Thin Solid Films* **515**, 3356 (2007).
- [21] M. Oikkonen, *J. Appl. Phys.* **62**, 1385 (1987).